NUWC-NPT Technical Report 11,316
15 October 2001

Stokes' Mechanism of Drag Reduction

Promode R. Bandyopadhyay
Torpedo Systems Technology Department

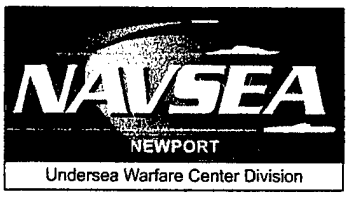

Naval Undersea Warfare Center Division
Newport, Rhode Island

PREFACE

This work was funded by the Office of Naval Research under grant (N0001499 WX30295), program manager Teresa McMullen (ONR 342).

The technical reviewer for this report was James L. Dick (Code 8233).

The author wishes to thank Teresa McMullen, whose support is gratefully acknowledged, and Kwing-So Choi for generously supplying his measurements and the flow visualization videotape. The author also wishes to thank Preetinder S. Virk for reviewing an early version of the work and his constructive criticisms, and Katepalli R. Sreenivasan, Garry L. Brown, John R. Grant, and James C. S. Meng for their comments.

Reviewed and Approved: 15 October 2001

Paul M. Dunn
Head, Torpedo Systems Technology Department

REPORT DOCUMENTATION PAGE

Form Approved
OMB No. 0704-0188

1. AGENCY USE ONLY *(Leave blank)*	2. REPORT DATE	3. REPORT TYPE AND DATES COVERED
	15 October 2001	

4. TITLE AND SUBTITLE

Stokes' Mechanism of Drag Reduction

5. FUNDING NUMBERS

6. AUTHOR(S)

Promode R. Bandyopadhyay

7. PERFORMING ORGANIZATION NAME(S) AND ADDRESS(ES)

Naval Undersea Warfare Center Division
1176 Howell Street
Newport, RI 02841-1708

8. PERFORMING ORGANIZATION REPORT NUMBER

TR 11,316

9. SPONSORING/MONITORING AGENCY NAME(S) AND ADDRESS(ES)

Office of the Chief of Naval Research
800 North Quincy Street
Ballston Centre Tower One
Arlington, VA 22217-5660

10. SPONSORING/MONITORING AGENCY REPORT NUMBER

11. SUPPLEMENTARY NOTES

12a. DISTRIBUTION/AVAILABILITY STATEMENT

Approved for public release; distribution is unlimited.

12b. DISTRIBUTION CODE

13. ABSTRACT (Maximum 200 words)

The mechanism of drag reduction due to spanwise wall oscillation in a turbulent boundary layer is considered in this report. Published measurements and simulation data are analyzed in light of Stokes' second problem. A kinematic vorticity reorientation hypothesis of drag reduction is first developed. It is shown that spanwise oscillation seeds the near-wall region with oblique and skewed Stokes' vorticity waves. They are attached to the wall and gradually align to the freestream direction away from it. The resulting Stokes' layer has an attenuated nature compared to its laminar counterpart. The attenuation factor increases in the buffer and viscous sublayer as the wall is approached. The mean velocity profile at the condition of maximum drag reduction is similar to that due to polymer. The final mean state of maximum drag reduction due to turbulence suppression appears to be universal in nature. Finally, it is shown that the proposed kinematic drag reduction hypothesis describes the measurements significantly better than the current direct numerical simulation method.

14. SUBJECT TERMS

Drag Reduction | Wall-Pressure Reduction | Limiting Drag Reduction | Stokes' Layer

15. NUMBER OF PAGES
33

16. PRICE CODE

17. SECURITY CLASSIFICATION OF REPORT	18. SECURITY CLASSIFICATION OF THIS PAGE	19. SECURITY CLASSIFICATION OF ABSTRACT	20. LIMITATION OF ABSTRACT
Unclassified	Unclassified	Unclassified	SAR

TABLE OF CONTENTS

LIST OF ILLUSTRATIONS

LIST OF ILLUSTRATIONS (Cont'd)

STOKES' MECHANISM OF DRAG REDUCTION

1. INTRODUCTION

Some of the recent developments in viscous drag reduction technology appear in the Proceedings of the International Symposium on Seawater Drag Reduction (reference 1). During the opening remarks at this meeting, VADM (Ret.) M. Firebaugh of Electric Boat Corp. emphasized that the subject remains extremely difficult. Passive methods, where no additive-like polymer or micro-bubble needs to be carried on board, are more desirable. The present interest in the method of superposing a spanwise wall oscillation, which applies to both air and water, arose in this light.

The discovery that the turbulence production in a boundary layer is not random and has an underlying quasi-cyclical nature has raised the hope that its control might be feasible; however, the development of drag reduction technology by means of turbulence suppression has been hampered by a lack of any well-founded theory. An attempt to control individual turbulence bursting is bound to be unrealistic in practice because the individual turbulence bursting numbers per unit area abound at higher Reynolds numbers. Moreover, individual turbulence bursting spatial and temporal locations cannot be predicted precisely.

Akhavan et al. (references 2 and 3), on the other hand, have carried out a direct numerical simulation (DNS) of a low-Reynolds-number, turbulent-channel flow where the wall was given a spanwise oscillation. They showed that, at certain oscillation frequencies that are non-dimensionalized by wall variables, the viscous drag was reduced substantially. This was a true prediction and, as such, a rarity. Two sets of subsequent experiments (references 4 and 5), carried out in turbulent boundary layers at low Reynolds numbers, have substantially verified the basic claim of Akhavan et al. Thus, this technique of turbulence suppression is in a unique position of being well-founded by a DNS simulation and experimental confirmation. An application of the approach is given in reference 6.

The mechanism of drag reduction by spanwise wall oscillation is not clear. There is speculation that a Stokes' mechanism is at play; however, no clear evidence of its existence is available. The modification of a laminar Stokes' mechanism in a turbulent environment also is not obvious. Most importantly, the manner by which any presumed Stokes' mechanism disrupts the normal turbulence production process needs to be understood. The purpose of this report is to provide these theoretical underpinnings to this technology.

2. RELEVANT PAST RESULTS

Stokes and Rayleigh (reference 7) have considered the linear harmonic oscillation of an infinite flat wall parallel to itself and in an infinite, otherwise undisturbed medium, given by $w = W\cos(ft)$. Here, $w(y,t)$ is fluid velocity at height y from the wall at time t, W is wall velocity, and $2\pi f$ is frequency. This is known as Stokes second problem. An exact solution of the Navier-Stokes equations for this flow can be obtained. When the non-dimensional, surface-normal distance is expressed as $\eta = y\sqrt{f/(2\upsilon)}$, the velocity profile is given by $w(y,t) = We^{-\eta}\cos(ft-\eta)$. The physical significance relevant to the present work is as follows: the spanwise oscillation imposes a perturbation that has a damped harmonic character away from the wall. Its amplitude is $We^{-\eta}$, and a fluid layer at distance y has a phase lag of η with respect to the motion of the wall, and a viscous wave of thickness $\propto \sqrt{\upsilon/f}$ is created.

The following tentative remarks can be made: because turbulence production in a turbulent boundary layer is basically a cyclical process, the superposed spanwise wall oscillation forces a lag on the near-wall fluid with respect to the wall, compared to what normally occurs in an unperturbed wall. This forced-phase mismatch between the incoming turbulent boundary layer and the wall has the potential to "misfire" the turbulence production trigger. However, the unabated flow of energy from the mean flow can be expected to manifest itself in the formation of some new near-wall waves, which do not occur in a normal, unperturbed turbulent boundary layer. The work done in creating these near-wall waves, known as Stokes' vorticity waves layer, may be considered as the penalty of this drag-reduction method.

Akhavan et al. have carried out the DNS simulation of a turbulent channel flow (references 2 and 3). The Reynolds number based on bulk velocity and channel-half width was 3000. When a spanwise oscillation of time period T_{osc} of 100 υ/U_τ^2 is imposed on the turbulent flow, a dramatic reduction in fluctuating vorticity near-wall was achieved, and the viscous drag was reduced by 40%. Here, U_τ is friction velocity. The results were essentially the same

whether it was the wall or the bulk fluid that was oscillated. The spanwise bulk fluid or wall velocity was 0.8 times the streamwise bulk velocity. Interestingly, at the same oscillation frequency, when the spanwise wall velocity was increased to 1.2 of the streamwise bulk velocity, the drag reduction increased to 50%. This suggested to Choi (reference 8) that a non-dimensional parameter, encompassing both spanwise oscillation frequency and velocity, governed the amount of drag reduction at a given Reynolds number, rather than $T_{osc}{}^{+}$ alone ($T_{osc}{}^{+} = \frac{T_{osc} U_{\tau}{}^{2}}{\upsilon}$).

The low-Reynolds-number true prediction of Akhavan et al. in a channel flow has been essentially verified by Laadhari et al. (reference 5) and Choi et al. (reference 4) in low-Reynolds-number turbulent boundary layers. This also indicates that the mechanism is a wall-layer phenomenon. Two plots of relevance to the present work are depicted in figures 1 and 2. Figure 1 shows the reduction in streamwise velocity (ΔU) near-wall. The velocities are non-dimensionalized by freestream velocity U_{∞} and the surface-normal distances are given in wall-layer coordinate y^{+}. The choice of U_{∞} as the velocity scale for ΔU is influenced by the apparent influence of the ratio of spanwise wall velocity to bulk flow velocity on drag reduction, as discussed in the previous paragraph. Figure 1 shows that the data do not collapse; i.e., U_{∞} is not the appropriate velocity scale and y^{+} is not the correct representation of length near-wall. There is a systematic variation with the frequency of wall oscillation f. It will be shown in this report that an appropriate scaling will improve the collapse in the data. Interestingly, the apparent scatter in the data at the lowest frequency of $f = 1\,Hz$ will also be eliminated. This examination of figure 1 indicates that the physics of the flow is not revealed by this format.

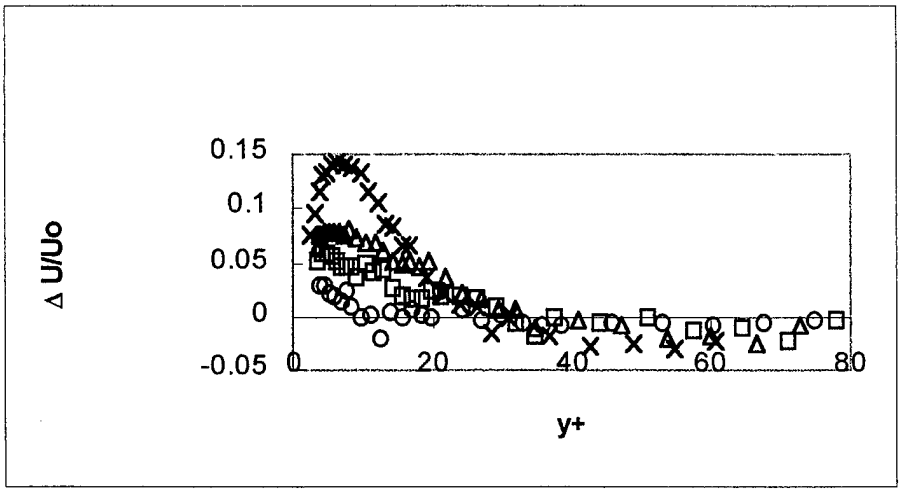

Figure 1. Measurements of Change in Axial Velocity Due to Spanwise Oscillation of a Turbulent Boundary Layer Normalized by Freestream Velocity (Symbols: O - 1 Hz; □ - 3 Hz; Δ - 5 Hz; and × - 7 Hz of wall-oscillation frequency. Figure reproduced from Choi et al. (reference 4).)

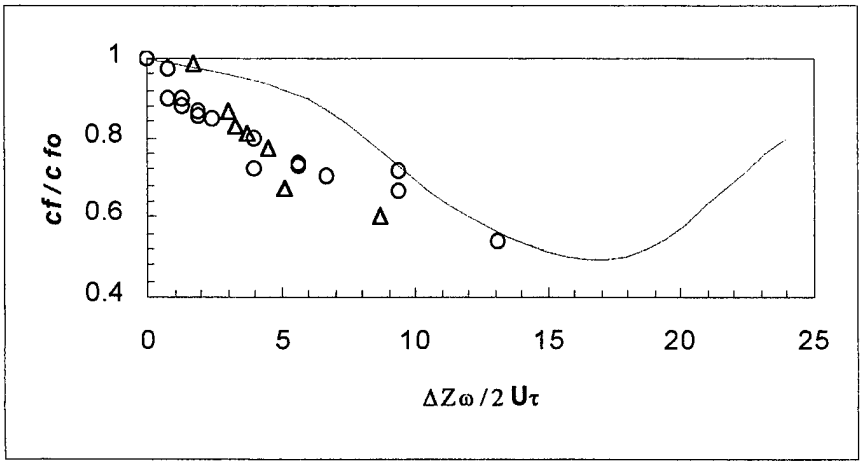

Figure 2. Comparison of Simulation and Measurements of Drag Reduction Due to Spanwise Wall Oscillation (reference 4) (Symbols are measurements in turbulent boundary layers: O - Choi et al. (reference 4); Δ - Laadhari et al. (reference 7); —— is DNS simulation in a channel flow dicovered by Akhavan et al. (reference 6). Figure reproduced from Choi et al. (reference 4).)

Figure 2 indicates the variation of reduction of skin friction with a new non-dimensional, wall-oscillation parameter $\frac{\Delta Z \varpi}{2U_\tau}$ discovered by Choi et al. (reference 4). Here, $\varpi = 2\pi f$ and ΔZ is the amplitude of the spanwise wall oscillation. The skin friction is measured after the oscillating wall. The value of this non-dimensional, wall-oscillation parameter is demonstrated by the fact that it leads to a good collapse of the two independent experimental data sets and a near-collapse with the DNS simulation. Note that Choi et al. have converted the DNS simulation data, which is time dependent, to allow a comparison with the experimental turbulent boundary layer, which is spatially developing.

In the following section, the near-wall flow mechanism due to the perturbed flow will be extracted from these measurements and Choi et al.'s flow visualization. This will lead to a clarification of the variation in the velocity reduction data in figure 1; a drag-reduction model will also be developed that will further reinforce the collapsing ability of Choi et al.'s parameter $\frac{\Delta Z \varpi}{2U_\tau}$ and provide a physical interpretation of it.

3. HYPOTHESIS OF DRAG REDUCTION: KINEMATIC REORIENTATION OF VORTICITY

It is hypothesized that spanwise wall oscillation causes a "partial slip" between the streamwise turbulent boundary layer flow and the wall that is the source of vorticity. This leads to a lower level of production and turbulence-induced viscous drag; this hypothesis is shown schematically in figure 3. Here ϖ_x represents the near-wall streamwise vortices that abound naturally in a turbulent boundary layer. The spanwise wall-oscillation imposes a wall vorticity of ϖ_z in the spanwise direction. The net vorticity ϖ is inclined at an angle of α to the flow direction. If c_{fo} is skin friction of the undisturbed boundary layer and c_f is the skin friction of the disturbed layer, then the reduction in viscous skin friction is given as follows:

$$c_f / c_{fo} = 1 - \beta Sin\alpha . \qquad (1)$$

Here β is the maximum reduction in skin friction that can be achieved purely by suppression of turbulence. Further drag reduction, for example, may be created from separation of the mean flow or the application of any body force; however, methods such as suction and injection are not being considered here. At this point, it is not clear how the value of β can be estimated; rather, from figure 2 it is assumed that $\beta = 0.5$. As shown in figure 3, drag reduction is zero when $\alpha = 0°$ and 180°, and it is at its maximum when $\alpha = 90°$ and 270°. It is implied that at $\alpha = 90°$ and 270°, all turbulence production is suppressed.

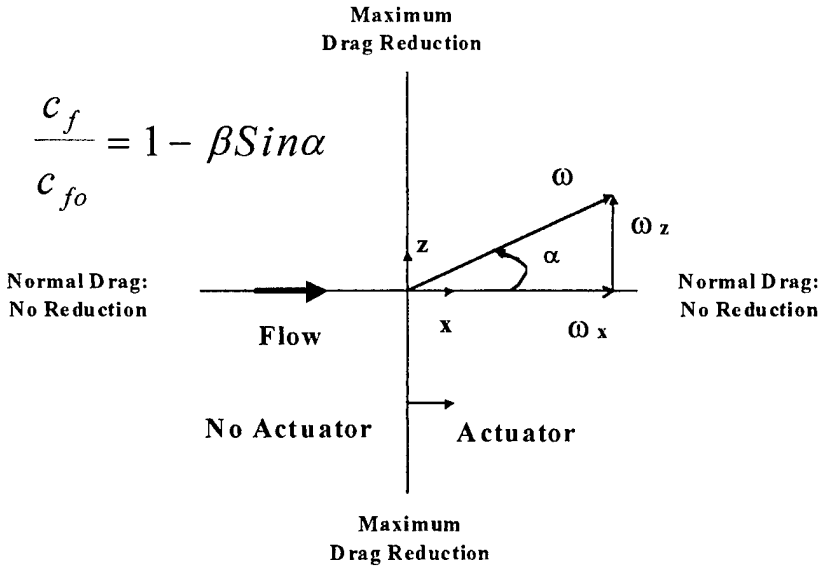

Figure 3. Schematic of Drag Reduction Hypothesis of Vorticity Reorientation

The relationship between drag reduction and vorticity reorientation angle α given by equation (1) is displayed in figure 4. A comparison with figure 2 shows that the decrease in drag reduction, predicted by the DNS simulation for values of Choi et al.'s wall-oscillation parameter $\frac{\Delta Z\varpi}{2U_\tau}$ greater than that for the condition of maximum drag reduction, is reproduced. A physical justification is also given by the hypothesis. However, a comparison of equation (1) with the experimental data and the simulation is premature because the relationship between the oscillation parameter $\frac{\Delta Z\varpi}{2U_\tau}$ and the vorticity reorientation angle α has not yet been established.

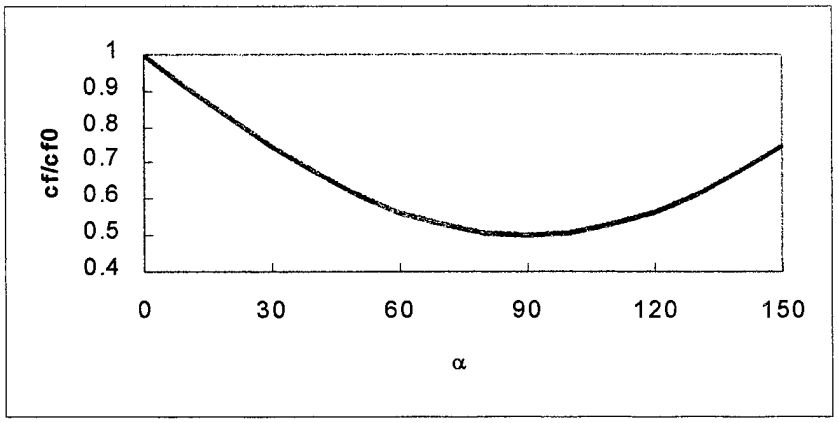

Figure 4. Drag Reduction Due to the Proposed Vorticity Reorientation Hypothesis

4. SCALES OF TURBULENT BOUNDARY LAYER (TBL) UNDER STOKES' PERTURBATION

First, the Stokes' layer-like behavior lying buried in the measurements of mean velocity profiles and in the flow visualization of the perturbed layer due to Choi et al. (reference 4) will be extracted. This will then be used to examine the state of the boundary layer at the condition of maximum drag reduction.

4.1 INNER-LAYER SCALES OF AN OSCILLATING TBL

Figure 1 shows that the spanwise oscillation has an effect on the mean streamwise velocity, which leads to a large reduction near the wall that changes over at $30 < y^+ < 50$ to a much smaller increase. It is unclear if this damped oscillatory behavior continues to another wavelength beyond $y^+ = 70$. It is reasonable to suspect that an appropriate scaling should reveal the Stokes' layer behavior lying nascent in this plot.

The velocity measurements, rather than the reductions, are plotted in figure 5 for an examination of the relevance of laminar Stokes' layer phase η. Measurements for all frequencies meet at $\eta = \pi/2$. This is encouraging because the presence of a damped oscillatory

phenomenon is implied. The effect of perturbation approaches an asymptotic distribution, indicating saturation as frequency is increased (a trend not highlighted in figure 1). Additionally, the relatively marked scatter at $f = 1\,Hz$ in figure 1 is no longer present. However, the distributions do not collapse at lower values of η. In fact, there is a strong and systematic effect of frequency. On hindsight, this is explained by noting that viscosity strongly attenuates the effect of the Stokes' mechanism near-wall. Therefore, when the velocity data are plotted in the normal wall-layer scales (figure 6), there is an excellent collapse up to $y^+ = 10$.

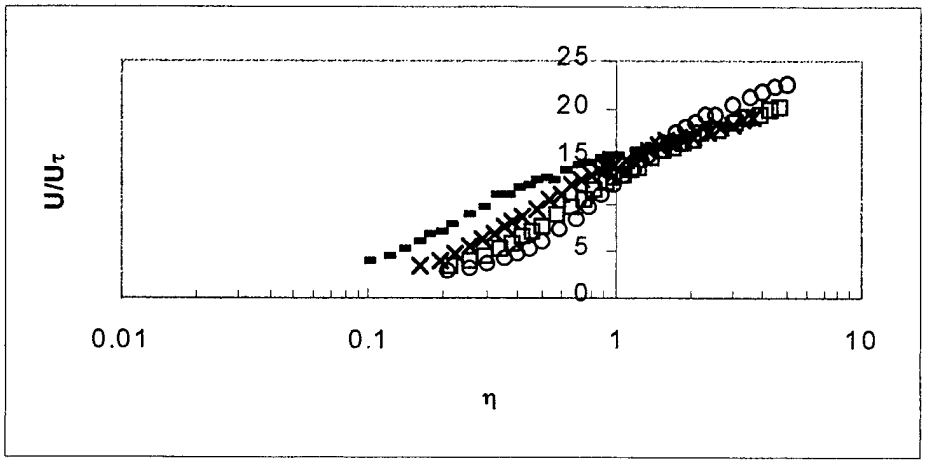

Figure 5. Stokes' Phase Variation of the Total Axial Velocity (Symbols: ▬ - 1 Hz; × - 3 Hz; □ - 5 Hz; O - 7 Hz. Measurements are proposed by Choi et al. (reference 4).)

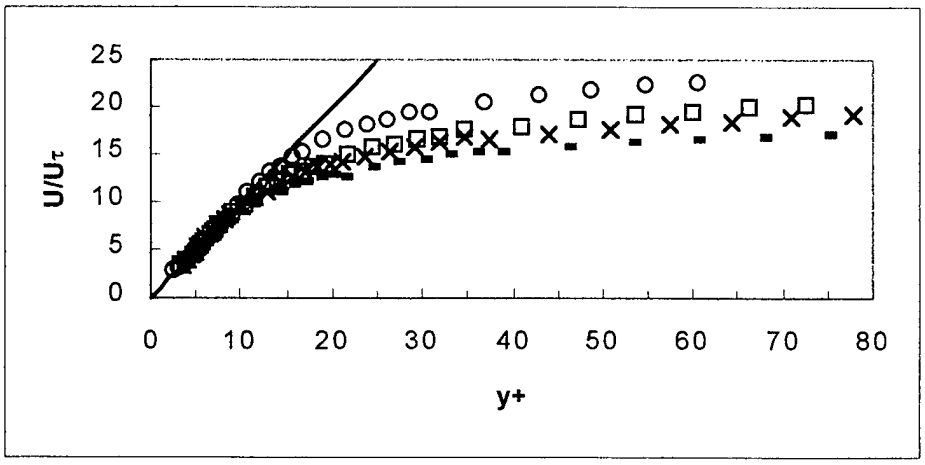

Figure 6. Total Axial Velocity in Normal Wall-Layer Velocity and Length Scales (Solid line is $U^+ = y^+$. Symbols ▬ - 1 Hz; × - 3 Hz; □ - 5 Hz; O - 7 Hz. Measurements are proposed by Choi et al. (reference 4).)

Figure 6 is replotted in the regular law-of-the-wall form in figure 7. Both figures 6 and 7 show that the collapse, up to about $y^+ = 10$, follows the viscous sublayer trend $U^+ = y^+$. Clearly, the thickness of the viscous sublayer has been increased, and in the case of $f = 7\ Hz$, has been increased nearly up to $y^+ = 13$. The mean velocity profile for the undisturbed flow is also included in figure 7.

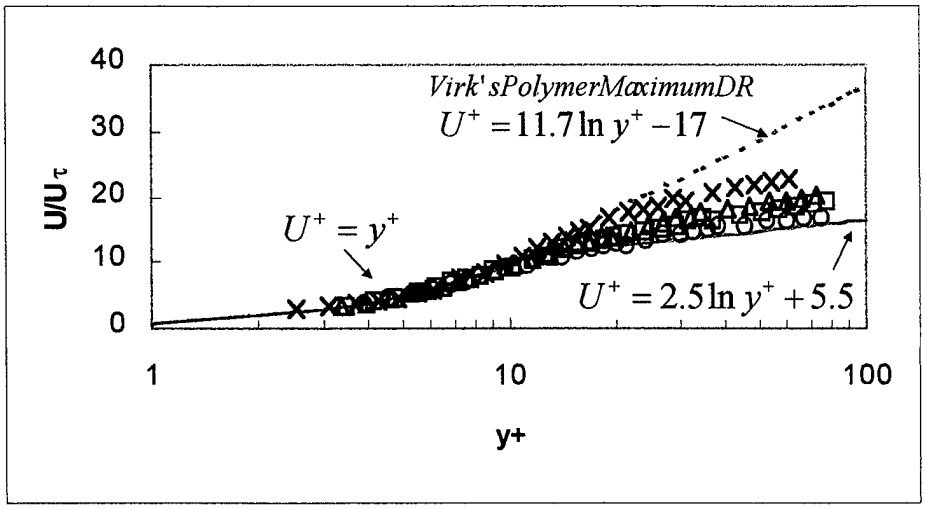

Figure 7. Regular Law-of-the-Wall Representation of the Effects of Increasing Frequency on Total Axial Velocity (The reference sublayer profile and the logarithmic velocity profile of unperturbed turbulent boundary layers are shown (——). Virk's (reference 9) ultimate polymer profile for the condition of maximum drag reduction is also shown (- - -). Symbols: o - 1 Hz; □ - 3 Hz; Δ - 5 Hz; x - 7 Hz. Measurements are proposed by Choi et al. (reference 4).)

The agreement with the sublayer profile up to $y^+ = 10$, and the approach to an asymptotic distribution at increasing frequencies of oscillation, encourage the comparison of the state of the mean velocity profile with that of Virk's (reference 9) polymer maximum drag reduction (PMDR), a profile of which is included in figure 7. Indeed, with increasing frequency of oscillation, the distributions approach the logarithmic PMDR profile, but they do not cross it. The distribution at $f = 7\ Hz$ approaches most closely, although it has not completely reached that state. This is in agreement with figure 2, where the maximum drag reduction in Choi et al.'s experiment falls short of the ultimate maximum drag reduction achievable by this technique, as indicated by Akhavan's et al.'s simulation.

4.2 ATTENUATION OF STOKES' LAYER

The exact nature of Stokes' layer is examined here. The change in streamwise velocity ΔU is scaled by the velocity scale of spanwise oscillation, namely $\Delta Z\varpi$, where ΔZ is the amplitude of the spanwise wall motion and ϖ is angular frequency $2\pi f$ (f being the frequency of the spanwise oscillation). This variable is plotted against Stokes' phase η in figure 8. The result is shown for f = *7, 5, and 3 Hz*. The f = *1 Hz* data are not yet included. Compared to figure 1, figure 8 indicates a better collapse, meaning that the wall-oscillation velocity scale does indeed describe the effect of oscillation.

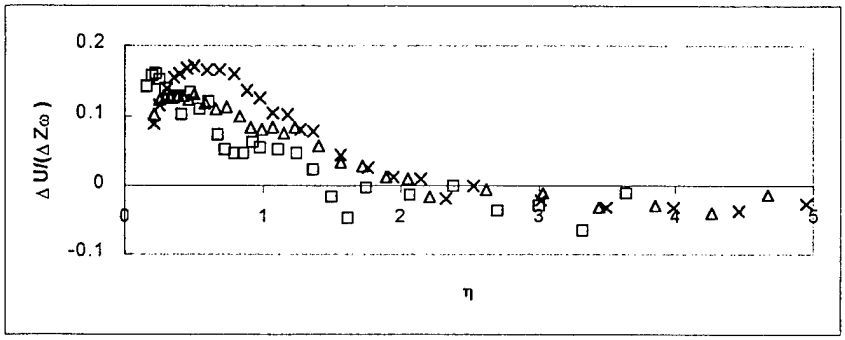

Figure 8. Stokes' Layer Scaling of Change in Axial Velocity Due to Spanwise Oscillation (Symbols: □ - 3 Hz; Δ - 5 Hz; x - 7 Hz. Measurements are proposed by Choi et al. (reference 4).)

Spanwise wall-motion effectiveness in imparting a spanwise displacement to the fluid in the ambience of a turbulent boundary layer is examined in figure 9. The displacement (Δz) of the smoke-marked fluid at distance y from the wall was measured from the flow-visualization video and is shown in the figure. The data do not follow the laminar Stokes' distribution. The mean data follow a similar damped oscillation distribution, but with an attenuation factor B of 3, rather than 1:

$$\Delta z / \Delta Z = e^{-B\eta}. \qquad (2)$$

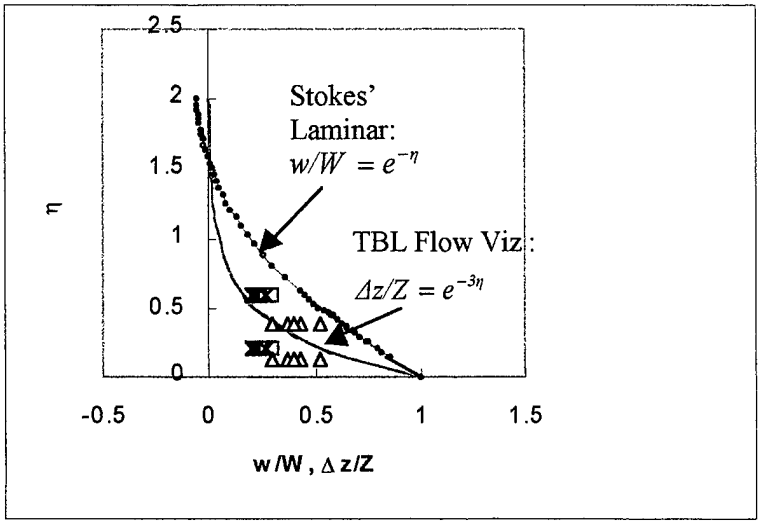

Figure 9. Stokes' Layer Phase Lag Representation of Spanwise Fluid Material Displacement (Symbols — and $\Delta z/Z$) in the oscillating turbulent boundary layer is compared with laminar Stokes' velocity profile (--•-- and w/W). Symbols: × - 5 Hz; □ - 5 Hz; and Δ - 2 Hz. The band in η indicates thickness of laser light sheet used for flow visualization. Data extracted from flow-visualization video by Choi et al. (references 4 and 8).)

The spanwise velocity scaling in figure 8 is reproduced in figure 10, where the $f = 1\ Hz$ data are now included. The damping of the effect on the axial velocity is compared with the general Stokes' layer relationship given by:

$$\Delta U/(\Delta Z \varpi) = e^{-B\eta} \cos(-B\eta). \qquad (3)$$

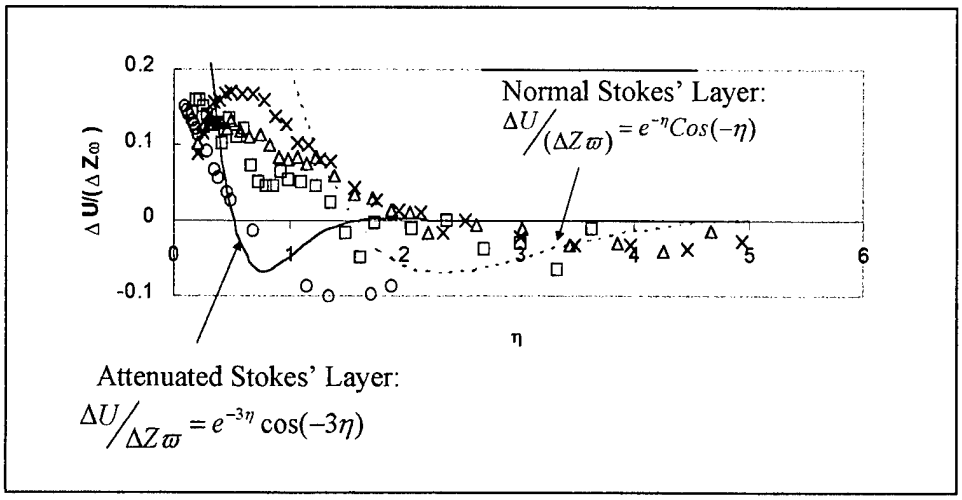

Figure 10. Attenuated Nature of Near-Wall Stokes' Layer in an Oscillating Turbulent Boundary Layer (Symbols: O - 1 Hz; □ - 3 Hz; Δ - 5 Hz; × - 7 Hz. Measurements were taken by Choi et al. (reference 4).)

The following trends may be observed: the Stokes' layer is actually attenuated and the attenuation factor is given by B. The scatter in the $f = 1\ Hz$ data seen in figure 1 is no longer present in figure 10. For lower values of η, the distribution for $f = 1\ Hz$ can be reasonably given by equation (3), where $B = 3$. At higher values, the normal Stokes' layer, where $B = 1$, is appropriate. At $f = 3, 5$ *and* $7\ Hz$ for $\eta > 1$, the damping given by $B = 1$ is valid. At $\eta = 1$ and $f = 3$ *and* $5\ Hz$, distributions show an interesting abrupt shift from high B values to $B = 1$; i.e., there appears to be a narrow band of phase η near 1, where the normal outer-layer of Stokes' layer merges with an attenuated near-wall Stokes' layer. In closing, the general observation is that Stokes' layer is normal ($B = 1$) for high values of η and is attenuated, with a variable attenuation factor, at lower values of η.

5. NEAR-WALL STRUCTURE OF TURBULENT BOUNDARY LAYER UNDER STOKES' PERTURBATION

In a quiescent ambient, the Stokes' mechanism of vorticity generation and transport away from the wall is well understood. How is this manifested in a turbulent boundary layer? The near-wall-flow visualization videotapes produced by Choi et al. (references 4 and 8) were examined to gain an insight. Downstream (> 100 wall units) of the oscillating/non-oscillating leading edge, it was observed that the flow in the viscous sublayer became organized, which happened just prior to the phase when the plate reached its either spanwise extreme position. (Note that this is when the plate had decelerated to a nearly zero speed.) The flow became organized into arrays of oblique two-dimensional and equi-spaced waves (figure 11). The appearance of such organization is striking because the instantaneous near-wall structure in the regular (non-oscillating) case is quite random. These waves should be attached to the wall; the implication is that they are most skewed at the wall, and gradually vanish away from it. The formation of these oblique waves provides some support to the vorticity reorientation hypothesis.

Figure 11. Oblique Two-Dimensional Stokes' Waves with Freestream Direction from Left to Right (Frame extracted from flow visualization video produced by Choi et al. (reference 4). Freestream velocity is 1.5 ms; wall-oscillation frequency is 5 Hz; amplitude of spanwise oscillation is 50 mm; figure is roughly in scale; height of laser light sheet is 1 ± 0.5 mm from wall.)

The relationship between vorticity reorientation angle and the oscillation parameter can be determined. Figure 2 shows that Choi et al. (reference 4) experiments came close but did not reach the condition for maximum drag reduction achievable, as given by an extrapolation of the experimental data or as predicted by DNS. Figure 12 shows the extrapolated frequency of wall-oscillation and friction velocity for maximum drag reduction in Choi et al.'s experiments based on equation (1) of the vorticity reorientation hypothesis. The following form of equation (1) is used:

$$U_\tau = U_{\tau o} - (U_{\tau o} - U_{\tau fmax}) Sin(0.5\pi f / f_{max}). \qquad (4)$$

Here, U_τ is friction velocity; subscript o stands for baseline unperturbed flow and *max* stands for the condition of maximum drag reduction. A best fit of equation (4) to data is sought. The wall-oscillation parameter for maximum drag reduction then turns out to be $\frac{\Delta Z \varpi}{2U_\tau} = 16.2$.

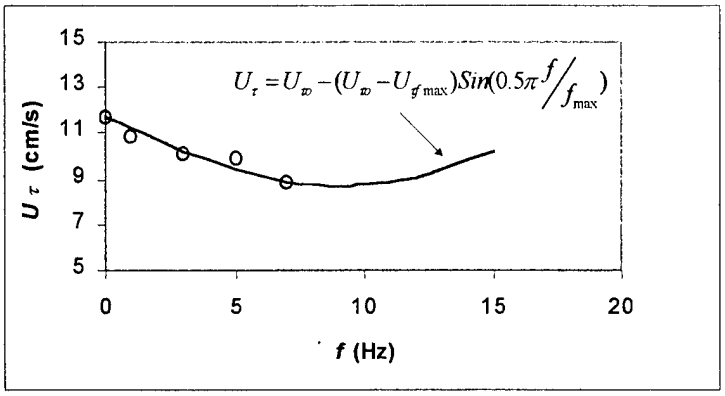

Figure 12. Extrapolation of Choi et al.'s (reference 4) Experimental Condition (Symbols) (This is carried out via proposed hypothesis of drag reduction (solid line) for the determination of the condition for maximum drag reduction.)

The relationship between vorticity reorientation angle and the oscillation parameter can now be obtained as shown in figure 13. The vorticity reorientation angle is 90° when $\frac{\Delta Z\varpi}{2U_\tau} = 16.2$, and 180° when $\frac{\Delta Z\varpi}{2U_\tau} = 32.4$. The solid line indicates this fact. The symbols are from the flow visualization of the oblique vorticity waves shown in figure 11. The attenuated Stokes' relationship shown in figure 9 is used to extrapolate the angles of Stokes' waves at the wall (α). There is agreement between the flow visualization symbols and the solid line representing the hypothesis.

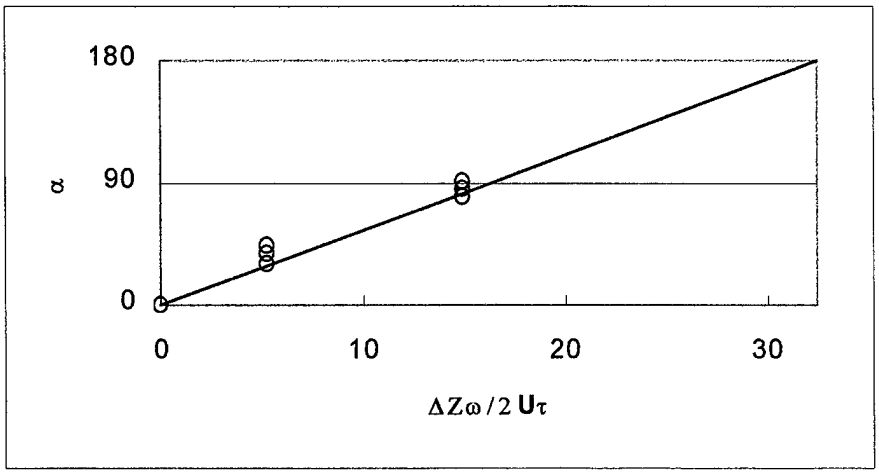

Figure 13. Relationship Between Vorticity Reorientation Angle and Choi et al.'s Oscillation Parameter (Symbols are from extrapolation of flow visualization data shown in figure 9 to the wall.)

6. UNIVERSAL MAXIMUM DRAG REDUCTION

It is understood that the routes to a complete suppression of turbulence are different in the Stokes' mechanism, and that is due to polymer injection. However, is the above-obtained condition for maximum drag reduction similar to that in Virk's polymer maximum drag reduction? This question is examined here in the context of mean velocity profile. In figures 6 and 7, it was shown that in the conditions of Choi et al.'s experiment, there was a collapse with the unperturbed viscous sublayer relationship $U^+ = y^+$, roughly up to $y^+ = 10$. Virk (reference

9) has reported a similar collapse due to polymer injection up to $y^+ = 11.4$. The question then is, in the extrapolated condition of maximum drag reduction obtained in figure 12, is the rest of the mean velocity profile identical to Virk's maximum drag reduction profile for polymer? To answer this question, the normal velocity profile for the unperturbed turbulent boundary layer in Choi et al.'s experiment was taken in U^+ versus y^+ form. The effect of the Stokes' layer can now be applied to it to determine the change in the mean velocity distribution. In figure 10, it was shown that in the outer part of the Stokes' layer, there is no attenuation and the normal value of $B = 1$ applies. Figure 14 shows that when the Stokes' layer effect is applied to the unperturbed profile and the friction velocity is obtained by the presently proposed vorticity reorientation relationship, Virk's polymer maximum drag reduction profile is recovered exactly. This strongly indicates that the mean velocity profile for maximum drag reduction is universal in nature, which is to be expected because if turbulence production is be truly suppressed, then the mean velocity profile has to be unique.

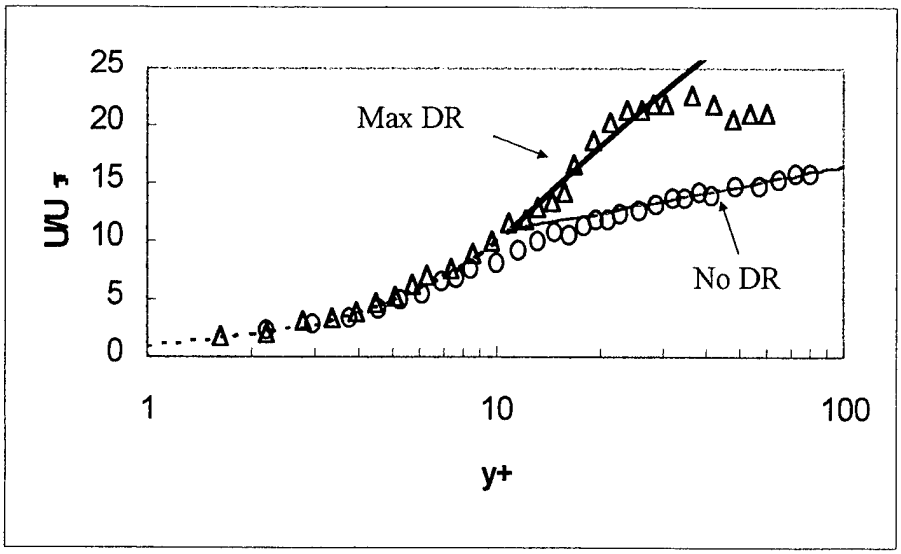

Figure 14. Recovery of Mean Velocity Profile for Maximum Drag Reduction from an Unperturbed Profile by Means of Attenuated Stokes' Layer Modeling (Symbols: O - unperturbed flow; Δ - computed maximum drag reduction. Broken and thick solid lines are Virk's polymer maximum drag reduction profiles (reference 9).)

In figure 10, the conclusion that $B > 1$ for lower values of η can now be better quantified. The attenuated Stokes' layer relationship in equation (3) was applied to the velocity profile for the unperturbed turbulent boundary layer shown in figure 14 to determine the value of B, which will allow the recovery of Virk's complete profile for polymer maximum drag reduction. The distribution of the required values of B is shown in figure 15. The value of B increases from 1 as the wall is approached in the buffer and viscous sublayer, where the effects of viscosity are also increasing. A more detailed analysis is required to understand this behavior.

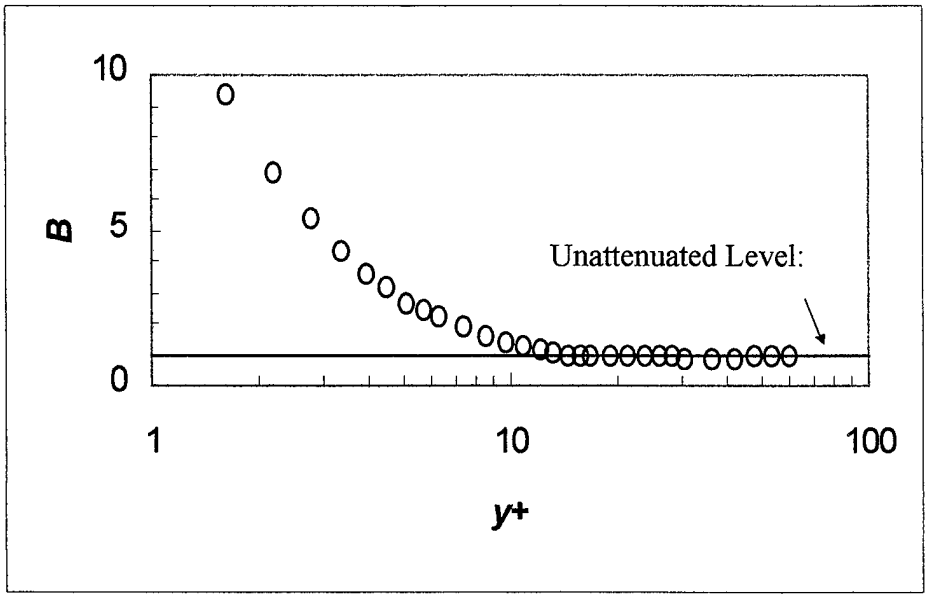

Figure 15. Calculated Variation of Stokes' Attenuation Parameter Across the Boundary Layer for the Condition of Maximum Drag Reduction

7. EVALUATION OF VORTICITY REORIENTATION HYPOTHESIS OF DRAG REDUCTION

The relationship between vorticity reorientation angle α and the spanwise oscillation parameter $\frac{\Delta Z\varpi}{2U_\tau}$ has been established in figure 13. This can now be utilized to compare the proposed drag reduction hypothesis shown in figure 4 with the summary of measurements and simulation shown in figure 2 (this comparison is shown in figure 16). The sine-wave model of the proposed hypothesis compares rather well with the experimental data; in fact, it does so better than the DNS simulation. It is suggested that the channel length has not been adequate in Akhavan et al.'s simulation (reference 3), and the slight disagreement can be cured if computations are repeated for a longer channel length (reference 8). The hypothesis can now be deemed as validated.

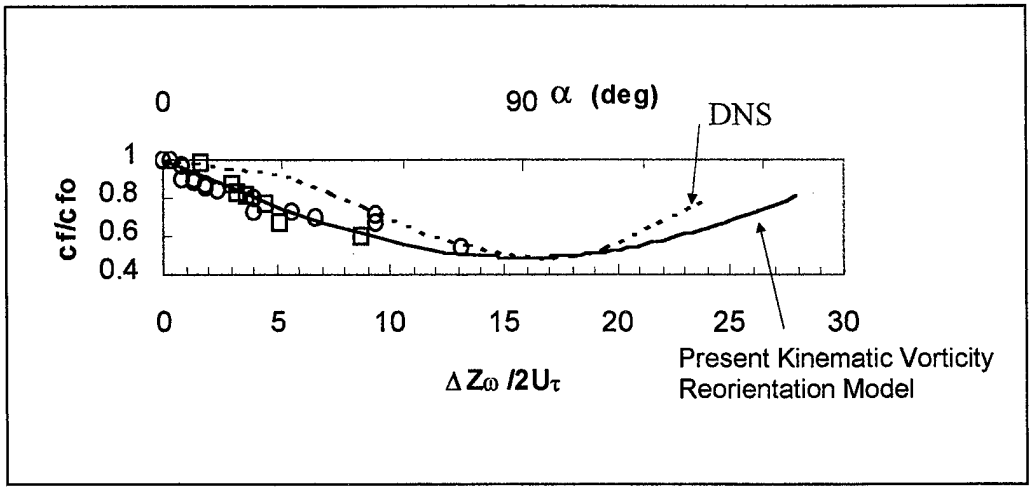

Figure 16. Validation of Vorticity Reorientation Hypothesis of Drag Reduction (Symbols are measurements in turbulent boundary layers: O - Choi et al. (reference 4) and □ - Laadhari et al. (reference 5); - - - is DNS simulation in a channel flow due to Akhavan (reference 3) and —— is presently proposed vorticity reorientation hypothesis.)

8. CONCLUSIONS

An investigation into Stokes' mechanism of drag reduction has been carried out. Available drag and mean velocity measurements from several investigators and flow visualization in low-Reynolds-number turbulent boundary layers, along with the DNS in low-Reynolds-number channel flows, have been analyzed. This has been undertaken in the framework of a vorticity reorientation hypothesis and the so-called Stokes' second problem. The following conclusions may be drawn:

- Stokes' mechanism of drag reduction has been elucidated. Its effect is to superpose a phase lag, albeit attenuated, which is compared to that in a Stokes' layer that is developing in a quiescent medium, between the wall and the turbulent boundary layer above it. This leads to an alteration of the normal phase relationship that exists between the quasi-cyclic processes that are responsible for the production of turbulence in an unperturbed turbulent boundary layer and the wall.

- Stokes' mechanism imposes an organized flow structure near the wall, and its effect scales with the representative velocity of spanwise wall motion. The spanwise wall-oscillation seeds the near-wall region of a turbulent boundary layer with oblique arrays of two-dimensional vorticity waves, which are attached to the wall with a gradually decreasing skew away from it.

- The mean velocity profile for the condition of maximum drag reduction is similar to that due to polymer drag reduction. This indicates that, when turbulence production is completely suppressed, the mean state of the boundary layer has a universal character that is independent of the mechanism or route to turbulence suppression.

- A kinematic sinusoidal vorticity reorientation model is shown to describe the drag reduction process.

9. REFERENCES

1. "Proceedings of the International Symposium on Seawater Drag Reduction," Naval Undersea Warfare Center, Newport, RI, 22-23 July 1998.

2. R. Akhavan, W.J. Jung, and N. Mangiavacchi, "Turbulence Control in Wall-Bounded Flows by Spanwise Oscillations," *Applied Scientific Research,* vol. 51, 1993, pp. 299-303.

3. W. J. Jung, N. Mangiavacchi, and R Akhavan, "Suppression of Turbulence in Wall-Bounded Flows by High-Frequency Spanwise Oscillations," *Physics of Fluids*, vol. A4, 1992, pp. 1605-1607.

4. K. S. Choi, J. R. DeBisschop, and B. R. Clayton, "Turbulent Boundary-Layer Control by Means of Spanwise-Wall Oscillation," *AIAA Journal of Spacecraft and Rockets*, vol. 36, pp. 1157-1163, 1998.

5. F. Laadhari, L. Skandaji, and R. Morel, "Turbulence Reduction in a Boundary Layer by a Local Spanwise Oscillating Surface," *Physics of Fluids*, vol. A6, pp. 3218-3220, 1994.

6. P. R. Bandyopadhyay, "A Nulled-Turbulence Aircraft and Underwater Vehicle," Navy Case # 79990, Patent Pending.

7. H. Schlichting, *Boundary-Layer Theory*, 7th Edition, MacGraw-Hill, New York, NY, 1978.

8. Private Communication with K. Choi, University of Nottingham, United Kingdom, Department of Mechanical Engineering, 1999.

9. P. S. Virk, "Drag Reduction Fundamentals," *American Institution of Chemical Engineers*, vol. 21, no. 4, pp. 625-656, 1975.

INITIAL DISTRIBUTION LIST

Addressee	No. of Copies
Naval Surface Warfare Center/Carderock Division (J. Fein, M. Donnelly, D. Hess)	3
Office of Naval Research (L. P. Purtell, K. Ng, T. McMullen, S. Lekoudis, W. S. Vaughan)	5
Naval Research Laboratory (W. Sandberg, R. Ramamurti)	2
NASA Langley Research Center (J.B.A. Anders, S. P. Wilkinson, L. M. Weinstein, W. Sellers, D. M. Bushnell)	5
Applied Research Laboratory (M. Billett, S. Deutsch)	2
University of California/San Diego (S. Sarkar)	1
University of California/Los Angeles (J. Kim)	1
University of Colorado/Boulder (S. Biringen)	1
Virginia Polytechnical Institute (D. P. Telionis, R. L. Simpson)	2
Cornell University (Z. J. Wang (App. Math), P. Stone, J. Lumley)	3
MIT/Department of Ocean Engineering (M. Triantafyllou, D. Liu, A. Annaswamy)	3
University of Houston (F. Hussain)	1
University of Michigan (G. M. Faeth, R. Akhavan)	2
University of Florida (Y. Hussaini, A. Krothapalli)	2
University of Southern California (R. Blackwelder)	1
University of Notre Dame (M. Gad-el-Hak)	1
University of Nottingham/United Kingdom (K. Choi)	1
University of Illinois (R. Adrian)	1
Princeton University (A. Smits, G. M. Brown, D. Nosenchuck)	3
Brown University (G. Karniadakis, K. Breuer)	2
Yale University (K. R. Sreenivasan)	1
Defense Technical Information Center	2
Center for Naval Analyses	1